

Lecture: Accelerator Physics
Winter 2024/25

Magnet Technology

Axel Bernhard

Contents

1	A brief guide to materials	3
1.1	Ferromagnetic materials	3
1.1.1	Permanent magnets	4
1.1.2	Soft magnetic materials	6
1.2	Superconductors	6
2	Undulator technology	9
2.1	Permanent magnet undulators	9
2.1.1	Pure Permanent Magnets (PPM)	9
2.1.2	Hybrid undulators	10
2.1.3	Excursus: PMU variants	11
2.2	Electromagnetic undulators	13
2.3	Transparency and field termination	17
2.4	Magnetic forces and mechanical requirements	18
2.5	Field Errors and their Correction	18
3	Multipole magnets	21
3.1	Basis: cylindrical multipole expansion	21
3.2	Iron-dominated multipole magnets	22
3.3	Coil-dominated multipole magnets	29

3 Multipole magnets

3.1 Basis: cylindrical multipole expansion

Assuming that there are no field sources in the vicinity of the beam, the following applies:

$$\text{rot } \vec{B} = 0$$

$$\Rightarrow \exists \text{ scalar potential } \Phi \text{ with } \vec{B} = -\text{grad } \Phi$$

For this potential, the *Laplace equation* applies

$$\Delta \Phi \equiv 0 \quad (3.1)$$

For electron beam dynamics, only solutions of the Laplace equation that are cylindrically symmetric around the beam axis are of interest.

Explicitly written in cylindrical coordinates, the Laplace equation is

$$\frac{\partial^2 \Phi}{\partial r^2} + \frac{1}{r} \frac{\partial \Phi}{\partial r} + \frac{1}{r^2} \frac{\partial^2 \Phi}{\partial \varphi^2} + \frac{\partial^2 \Phi}{\partial s^2} \equiv 0 \quad (3.2)$$

In a first approximation, the magnetic grid is represented by piecewise solutions of the Laplace equation in s constant solutions. This is the so-called *hard-edge approximation*.

Usually, for the description of beam-steering magnets, the transverse coordinates and thus also the potentials and field components in the transverse direction are written as complex numbers.

The Laplace equation is fulfilled in this notation by piecewise in s constant potentials in the form of a Taylor expansion around the reference orbit $r = 0$ (multipole expansion)

$$\Phi(r, \varphi, s) = \sum_{n>0} \Phi_n(r, \varphi) \quad (3.3)$$

with

$$\begin{aligned} \Phi_n(r, \varphi) &= -\frac{p}{e} \frac{1}{n!} A_n r^n e^{in\varphi} \\ \Phi_n(x, y) &= -\frac{p}{e} \frac{1}{n!} A_n (x + iy)^n \end{aligned} \quad (3.4)$$

and

$$A_n = \left. \frac{\partial^{n-1} B_y}{\partial x^{n-1}} \right|_{\substack{x=0 \\ y=0}} \quad (3.5)$$

(The reader can convince himself of this by substituting into the Laplace equation).

The real and imaginary parts of these potentials represent two linearly independent solutions of the Laplace equation

$$\text{Re}(\Phi_n), \text{Im}(\Phi_n).$$

The imaginary solutions of the Laplace equation have the property

$$\text{Im}(\Phi_n)(x, y) = -\text{Im}(\Phi_n)(x, -y) \Rightarrow B_{ny}(x, y) = B_{ny}(x, -y)$$

i.e. they exhibit mirror symmetry with respect to the midplane. These multipoles are referred to as *perpendicularly* oriented multipoles.

In contrast, the real solutions represent the *rotated* multipoles.

The rotated multipoles of order n are rotated by $\frac{\pi}{2n}$ around the beam axis.

Remark. The rotated multipoles cause a coupling between the dynamics in the x and y directions. The perpendicular ones do not do this, at least for particles in the centre planes. In optics consisting of perpendicular dipoles and quadrupoles, the dynamics in the x and y directions are even completely decoupled. Therefore, beam transport systems are usually built (mainly) from perpendicular magnets.

3.2 Iron-dominated multipole magnets

The basic two-dimensional (transverse) design of iron-dominated multipole magnets is based on the fact that the field lines of the magnetic flux density on the surface of highly permeable pole materials are perpendicular, and the sections of the pole surfaces with the $x - y$ plane are therefore equipotential lines of the scalar magnetic potential.

Pole shapes of pure multipole magnets

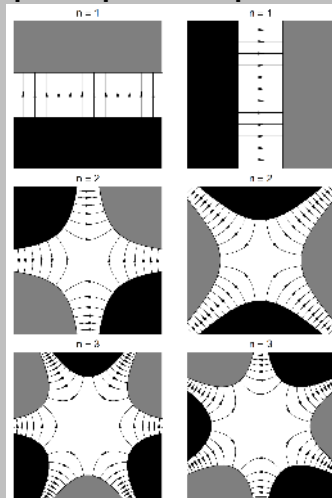


Figure 8: Pole shapes for iron-dominated magnets of the first three multipole orders, vertical and rotated. (Fig.: A. Wolski in Brandt 2010)

The field strength of a multipole magnet as a function of the number of Ampère-turns can be determined by applying Ampère's law

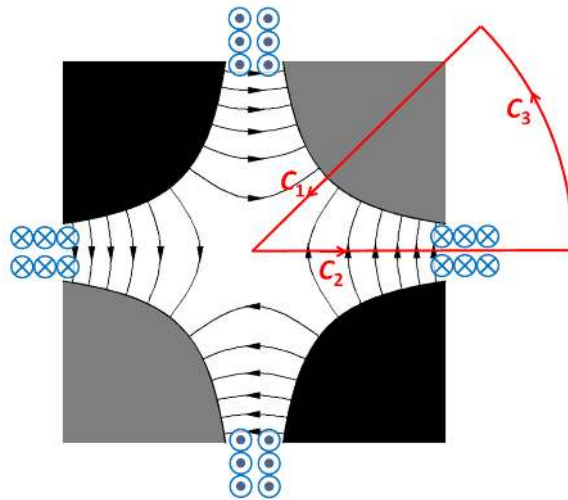


Figure 9: Integration path for determining the multipole strengths (Fig: A. Wolski in Brandt 2010)

$$\int_{C_1} \vec{H} d\vec{l} + \int_{C_2} \vec{H} d\vec{l} + \int_{C_3} \vec{H} d\vec{l} = -NI, \quad (3.6)$$

with the result for

$$\begin{aligned} \text{a dipole: } B_y &= \frac{\mu_0 NI}{g} \\ \text{a quadrupole: } \frac{\partial B_y}{\partial x} &= \frac{2\mu_0 NI}{r_0^2} \end{aligned} \quad (3.7)$$

with the gap height of the dipole g and the pole radius of the quadrupole r_0 , respectively.

This can be generalised for arbitrary multipoles of order n to

$$B_y + iB_x = \frac{\mu_0 n NI}{r_0} \left(\frac{x + iy}{r_0} \right) \quad (3.8)$$

Types of dipole magnets

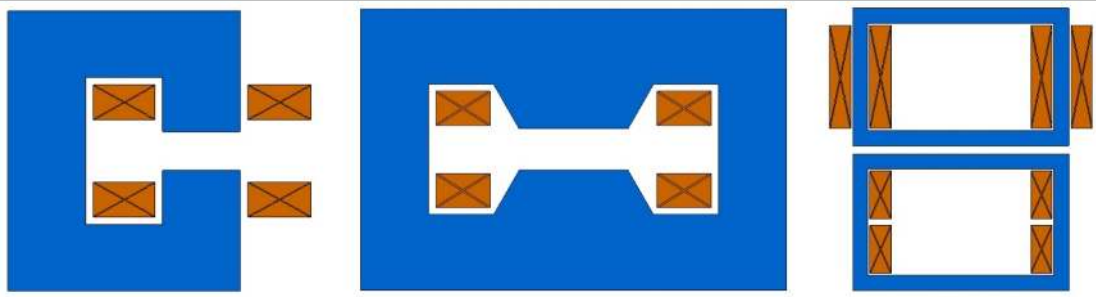


Figure 10: Typical designs for dipole magnets: C-magnet, H-magnet and window-frame designs (Fig.: Th. Zickler in Brandt 2010)

Types of quadrupole magnets

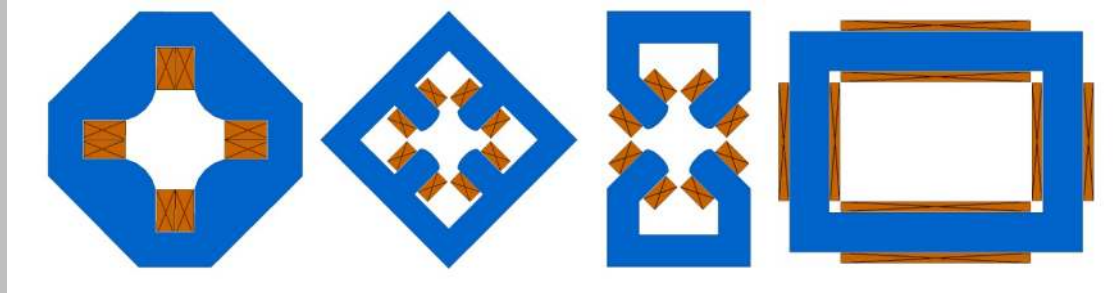


Figure 11: Typical designs for quadrupole magnets (Fig: Th. Zickler in Brandt 2010)

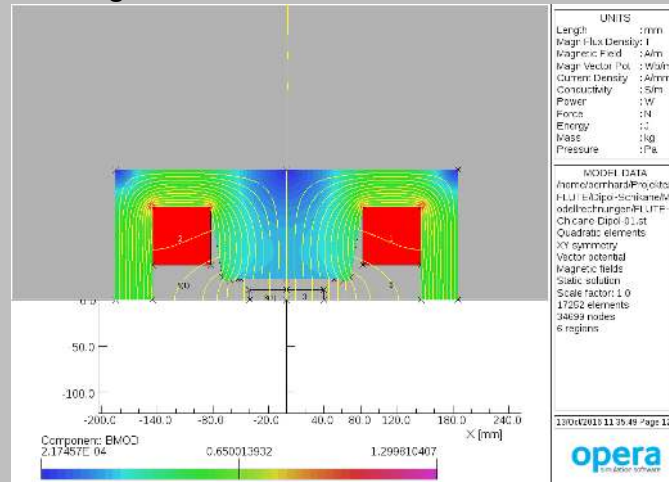
A practical example: design of the dipoles for the FLUTE bunch compressor

A practical example: dipoles for the FLUTE bunch compressor

Basic target parameters and specifications

electron energy	MeV	40–50
deflection angle		(0-15)°
magnet pole shape		rectangular
magnet type		H, movable
magnet length (geometric)	mm	200
max. magn. flux density	mT	220
good field width ($ \Delta B_y/B_{y0} \leq 10^{-4}$)	mm	74,6 (optimisation for 80)
gap width	mm	45
Ampère-Turns		7878
current density	A mm ⁻²	1

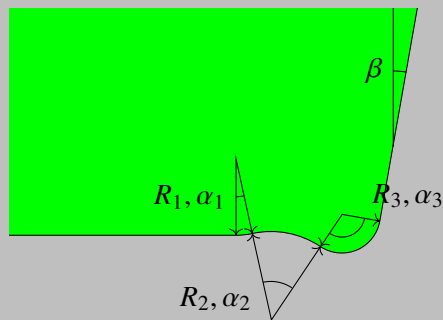
2D design



Parameterised model

- quadratic coil cross section 7878 mm^2
- pole shape avoiding flux density peaks at edges
- 3-bump shims reducing required pole overhang

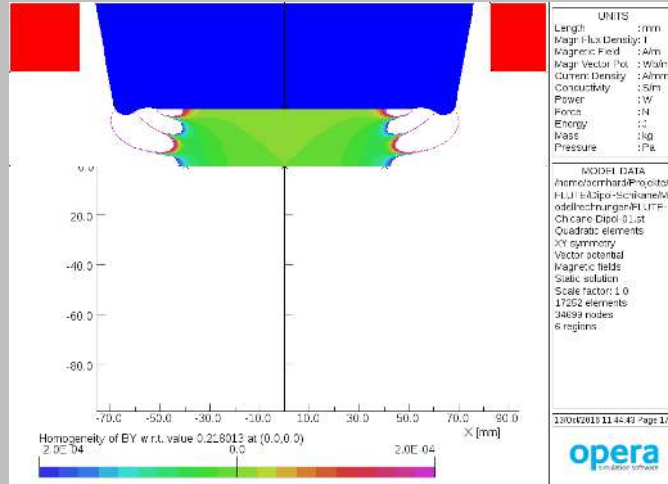
2D design detail: shim geometry



Optimisation

- Fixed parameters: flat pole width W_p , pole angle β
- Free parameters: bump radii R_1, R_2, R_3 , bump angles α_1, α_2
- minimize $M = \frac{|B_y - B_y(0,0)|}{B_y(0,0)}$ for (x, y) in region $x \in [-40 \text{ mm}; 40 \text{ mm}]$, $y \in [0; 10.5 \text{ mm}]$
- success criterion: $M \leq 1 \times 10^{-4}$

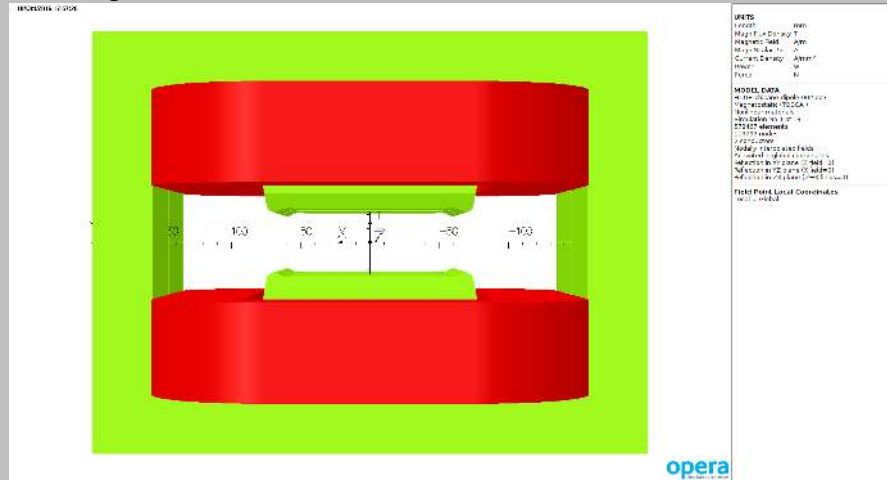
2D design: optimisation results

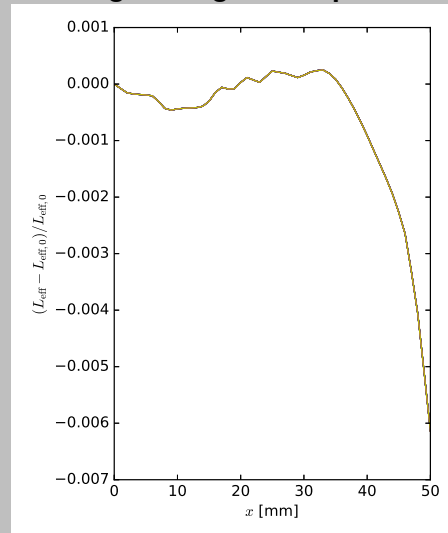


Successful minimisation

fixed	
W_p	100 mm
β	10°
optimised	
R1	10.14 mm
α_1	12.25°
R2	11.69 mm
α_2	46.10°
R3	5.11 mm
resulting	
$B_y(0,0)$	218 mT

3D design



3D design: Fringe field optimisation**Conclusion**

- relative variation of L_{eff} can be pushed below 0.1 % for a large part of the desired good-field region
- however, L_{eff} rapidly drops for $x > 35$ mm
- flat pole width seems to small
- complete optimisation procedure repeated for 55 mm flat pole width

Electric Power

The electric power dissipated in the magnet coils is

$$P = J^2 \rho_{\text{Cu}} V_{\text{Cu}}$$

$$= \frac{1}{A_{\text{Cu}}/A_{\text{eng}}} J_{\text{eng}}^2 \rho_{\text{Cu}} V_{\text{eng}}.$$

$A_{\text{Cu}}/A_{\text{eng}}$ depends on the choice of the conductor and takes into account insulation, packing factor and cross section of water cooling channels.

A reasonable lower limit of this factor can be estimated for both, water and air-cooled coils:

$$\frac{A_{\text{Cu}}}{A_{\text{eng}}} \geq 0.65 \quad (3.9)$$

Result:

Magnet length	200 mm	150 mm
Power per coil	101 W	91 W

3.3 Coil-dominated multipole magnets

The fields of coil-dominated magnets result from the arrangement of the current-carrying elements with Ampère's law or Biot-Savart.

We approach the coil-dominated pure multipole magnets via the rather academic model of a distribution of axis-parallel currents on a cylindrical surface.

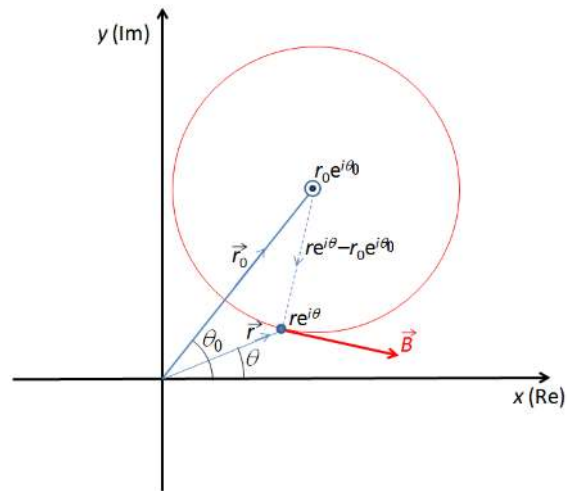


Figure 12: Coordinate system in the complex plane for describing the current distribution and the magnetic field of a coil-dominated magnet (Fig: A. Wolski in Brandt 2010)

Cylindrical surface with a cylinder radius r_0 . Current distribution on the cylindrical surface of the form

$$I(\theta_0) = I_0 \cos(n_0\theta_0 - \phi) \quad (3.10)$$

$$\Rightarrow B_y + iB_x = -\frac{I_0}{2\pi\mu_0 r_0} \left(\frac{r}{r_0}\right)^{n_0-1} e^{i(n_0-1)\theta} \pi e^{-i\phi}, \quad (3.11)$$

i.e. a cosinusoidal current distribution produces a pure multipole.

Multipole due to cosinusoidal current distribution

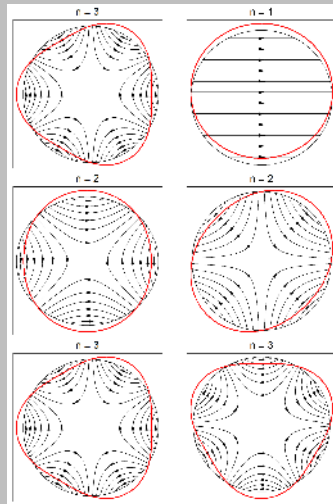


Figure 13: Ideal azimuthal current distribution and field lines of the resulting field distribution for the first three multipole orders (Fig: A. Wolski in Brandt 2010)

Real coil geometries approach this current distribution.

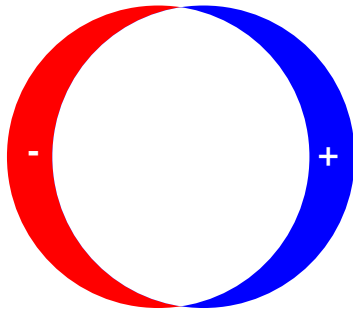
A current distribution on a cylinder is of course not feasible in reality. Instead, a corresponding current distribution must be realised using coils with constant current density. Such arrangements can be approximated with another model, the intersection of two conductors with elliptical cross-sectional area (half-axes a_i and b_i , $i = 1, 2$, centred at $\pm x_0$) and the same current density J of opposite sign:

Inside such conductors,

$$B_{xi} = \mp \mu_0 J \frac{a_i}{a_i + b_i} y, \quad B_{yi} = \pm \mu_0 J \frac{b_i}{a_i + b_i} (x \pm x_0) \quad (3.12)$$

Field in the interface:

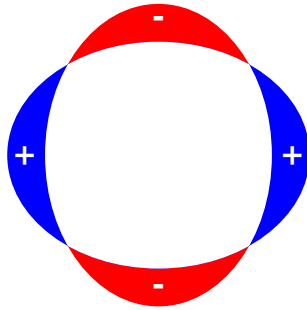
Case 1: $a_1 = a_2 = a$, $b_1 = b_2 = b$, $x_0 = c/2$:



$$B_x = 0, \quad B_y = \mu_0 J c \frac{b}{a+b} = \text{const.} \quad (3.13)$$

Dipole

Case 2: $a_1 = b_2 = a, a_2 = b_1 = b, x_0 = 0$:



$$B_x = \mu_0 J \frac{b-a}{b+a} y, \quad B_y = \mu_0 J \frac{b-a}{b+a} x \quad (3.14)$$

Quadrupole

Real coil geometries approximate these model distributions.

Coil block geometries for coil-dominated dipoles

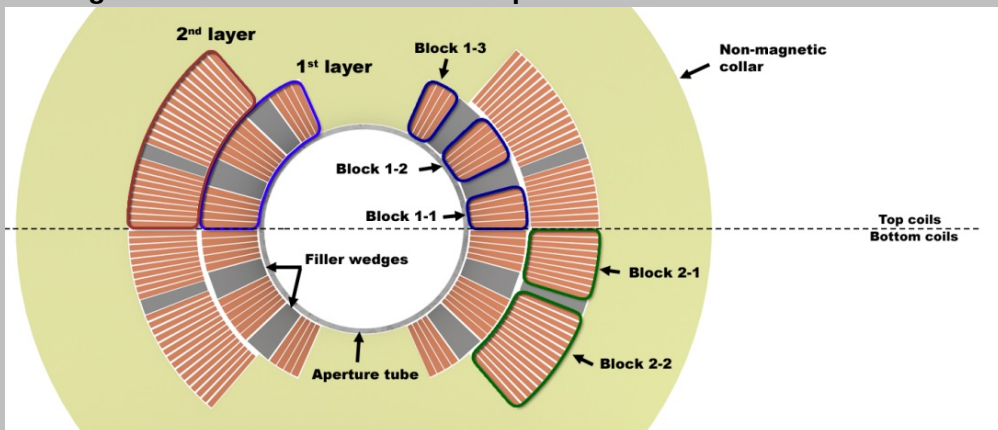


Figure 14: Cross-section of a $\cos \vartheta$ dipole (Fig.: Charlie Sanabria, CC-BY-4.0 Sanabria 2017)

3D arrangement of cosine-theta coils

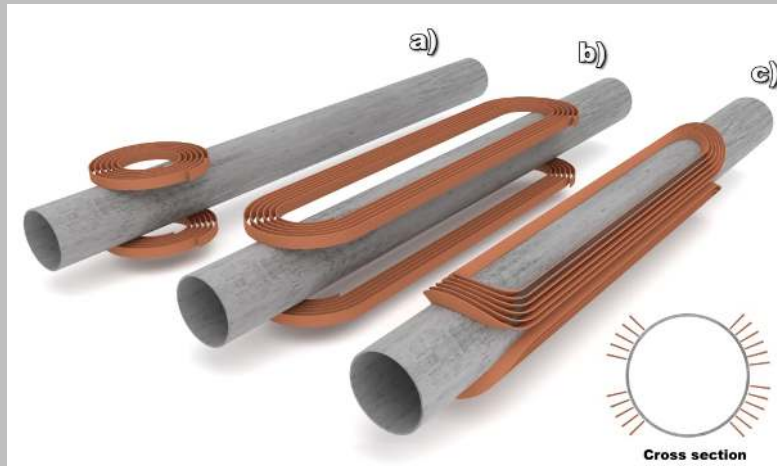


Figure 15: Principle of the end coil design of coil-dominated magnets (Fig.: Charlie Sanabria, CC-BY-4.0 Sanabria 2017)

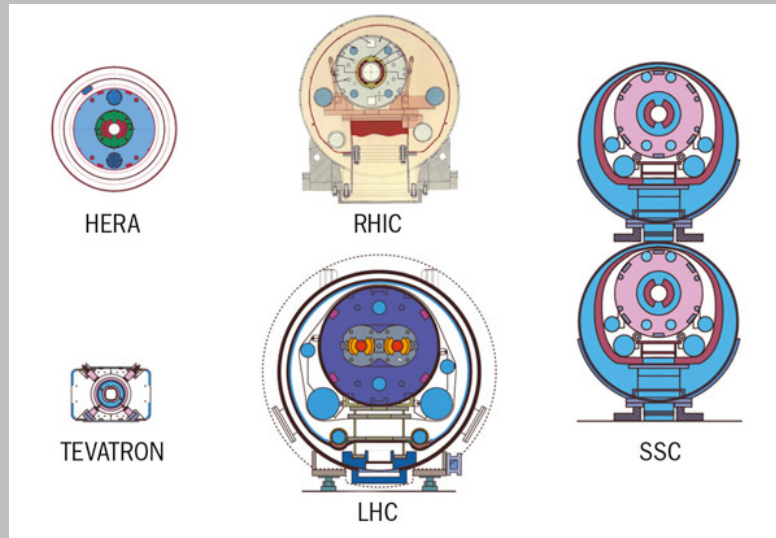
The fields that can be achieved with coil-dominated magnets scale with the achievable current density. Since this is 400 (air-cooled coils) to 100 times (water-cooled coils) higher for superconducting magnets than for normal conductors, coil-dominated magnets are the domain of superconductivity.

Remark. For the dipole case, it is instructive to rearrange the equation and relate it to the critical current density or the critical field B_{c2} :

$$B = \mu_0 \lambda d (B_{c2} - B) c \frac{b}{a + b} \quad (3.15)$$

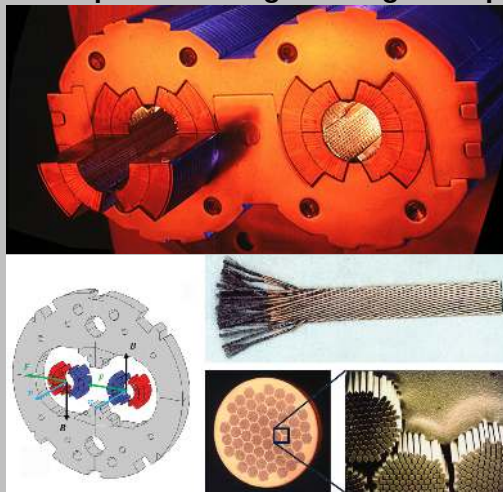
with λ the filling factor and $d = - \left. \frac{dJ_c}{dB} \right|_{B_{c2}}$.

On the one hand, it can be said that the achievable field strength scales with the coil thickness c and the critical current density. The rearranged equation also shows: for $B \rightarrow B_{c2}$ $c \rightarrow \infty$ must be aimed for. Consequently, the key to higher fields lies in increasing B_{c2} .

Examples

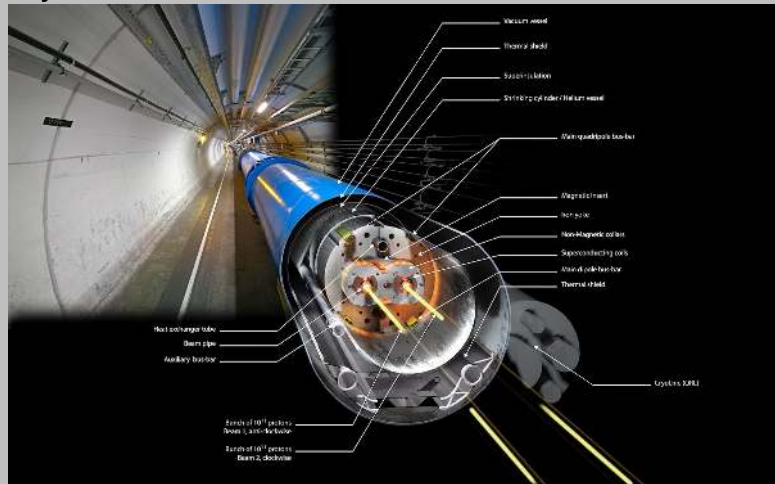
source: *Taking a Closer Look at LHC - Magnetic Dipoles* 2020

Tevatron: 4 T HERA 6 T SSC 6.6 T LHC 8.65 T HiLumi upgrade: 11 T FCC: 16 T

LHC dipole: two neighbouring beam pipes

- 2 pairs of coils, each with 80 Rutherford cables with 6500 filaments each
- with 1232 dipoles per 15 m in length, that adds up to 1.4×10^{12} m of superconducting filaments
- transport current per cable: 11.8 kA
- magnetic force on each coil: $2 \times 10^6 \text{ N m}^{-1}$
- field energy per dipole: 7 MJ

source: *Taking a Closer Look at LHC - Magnetic Dipoles* 2020

LHC-Dipole: cryo module

source: Brice 2011

References

Brandt, Daniel, ed. (2010). *Proceedings / CAS CERN Accelerator School Magnets: Bruges, Belgium, 16 - 25 June 2009*. CERN 2010,4. Geneva: CERN. 486 pp. ISBN: 978-92-9083-355-0.

Brice, Maximilien (2011). *Cross Section of an LHC Dipole in the Tunnel*. URL: <http://cds.cern.ch/record/1365795>.

Sanabria, Charlie (2017). *Restacked Rod Process Thesis Work - MagLab*. URL: <https://nationalmaglab.org/magnet-development/applied-superconductivity-center/asc-image-gallery/restacked-rod-process-thesis> (visited on 07/18/2019).

Taking a Closer Look at LHC - Magnetic Dipoles (2020). URL: https://www.lhc-closer.es/taking_a_closer_look_at_lhc/0.magnetic_dipoles (visited on 02/06/2020).